Potential Structures and Flow Measurements with Separatrix Biasing in the CASTOR Tokamak

VAN OOST Guido*, STÖCKEL Jan[1], HRON Martin[1], DEVYNCK Pascal[2], DYABILIN Konstantin[3], GUNN Jamie[2], HORÁČEK Jan[1], MARTINES Emilio[4] and TENDLER Michael[5]

Department of Applied Physics, Ghent University, Belgium

[1]*Institute of Plasma Physics, Prague, Czech Republic*

[2]*DRFC, CEA-Cadarache, France*

[3]*Institute for High Energy Densities, Moscow, Russia*

[4]*Consorzio RFX, Padova, Italy,*

[5]*Alfvén Laboratory, Royal Institute of Technology, Stockholm, Sweden*

Abstract

The impact of sheared electric fields on the structure of edge fluctuations and plasma flows is investigated on the CASTOR tokamak. A non-intrusive biasing scheme is applied, whereby the electrode is located in the SOL, but its top is just touching the separatrix. There is evidence of a strongly sheared radial electric field and formation of a transport barrier at the separatrix. The $E \times B$ shear rate is larger than for edge plasma biasing. It significantly exceeds the typical growth rate of unstable modes and has a strong impact on the turbulent structures, as demonstrated by Langmuir probe array measurements. Plasma flows, measured by a fast rotating Mach probe, are strongly affected in the sheared region, in particular in the perpendicular direction.

Keywords:

1. Introduction

It has been demonstrated on many machines with a variety of discharge- and heating conditions as well as edge biasing schemes that $E \times B$ flow velocity shear is a robust and universal mechanism to reduce plasma turbulence and to establish transport barriers. The CASTOR edge biasing arrangement and novel diagnostics have recently contributed to the improved understanding of the physical mechanisms involved. On CASTOR, the biased electrode can be located at two different positions with respect to the separatrix: *"Standard" configuration of biasing experiments*: The electrode is located deep in the edge plasma, i.e. in the region with closed magnetic field lines. Consequently,

the sheared radial electric field is amplified between the electrode and the separatrix. Although, this arrangement has contributed significantly on different machines to reveal the key role of electric fields, see e.g. [1-3], it can hardly be accepted in practice in large-scale experiments with high thermal loads.

Biasing of separatrix: Alternatively, the biased electrode is inserted just into the scrape-off layer (SOL) [4]. In this case, the thermal load on the electrode should certainly be smaller than in the previous case and such scheme can be employed as non-intrusive one. It was suggested [5] that separatrix biasing (i.e. imposing a boundary condition on the separatrix) is an efficient way

---

Corresponding author's e-mail: g.vanoost@fz-juelich.de

to create strongly sheared electric fields, thereby affecting plasma flows and turbulent structures. The boundary condition is governed by the electric field within the SOL, and L-H transition is triggered provided that the electric field on the separatrix has been raised significantly above the neoclassical value.

In this contribution we report on the sheared flow decorrelation of turbulent structures by modifying the radial electric field in the edge plasma. The biasing set-up and the novel diagnostics are described in Sec 2 and 3, respectively. Plasma flow and turbulence measurements are discussed in Sec 4. Conclusions are drawn in Sec 5.

2. Set-Up of Biasing Experiments

The impact of sheared electric fields on the turbulent structures and plasma flows is investigated on the tokamak CASTOR (R = 0.4 m, a = 0.085 m) at B_t = 1 T, I_p = 9 kA (i.e. high q operation) and line averaged densities $\bar{n}_e$ = 1·10^{19} m^{-3}. In the plasma edge, the density is in the range of 0.5 ÷ 2·10^{18} m^{-3} and the electron temperature is between 10 ÷ 20 eV. A mushroom-like biasing electrode (made of carbon) is inserted into the plasma from the top of the torus and biased with respect to the vacuum vessel by a pulsed voltage.

It has been found on the CASTOR tokamak that separatrix biasing is effective only if the SOL is broader than the radial extent of the biasing electrode. For this purpose, the plasma column is shifted downwards, as schematically shown in Fig. 1. Therefore, the minor radius of the plasma column is not determined by the radius of the poloidal limiter, but is reduced to $a - \Delta$. As a consequence, the SOL becomes broader (width 2Δ) at the top of the torus. The connection length in this region is long compared to the circumference of the torus (2π R).

As seen from the figure, the mushroom electrode is hidden in the SOL and its top is just touching the separatrix. The location of the separatrix (the last closed flux surface) is not determined by magnetic diagnostics on CASTOR, but is taken as the position of the velocity shear layer (VSL) where the radial electric field and the poloidal flow velocities are measured to be zero. The VSL position is deduced from the floating potential profile, measured by the rake probe in every shot. The radial position of the separatrix can vary within several mm, depending on the discharge conditions.

Because of the strong poloidal asymmetry of the scrape-off layer (SOL), the main diagnostics of the biasing experiment are located at the same poloidal

angle as the electrode, i.e. at the top of the torus.

3. Diagnostics

The edge plasma is diagnosed on CASTOR by electrical probes. Some of them (such as the rake probe and the poloidal probe array) were already described earlier [6]. Here, we present two novel diagnostics to investigate plasma flows and properties of turbulent structures in the radial and poloidal direction.
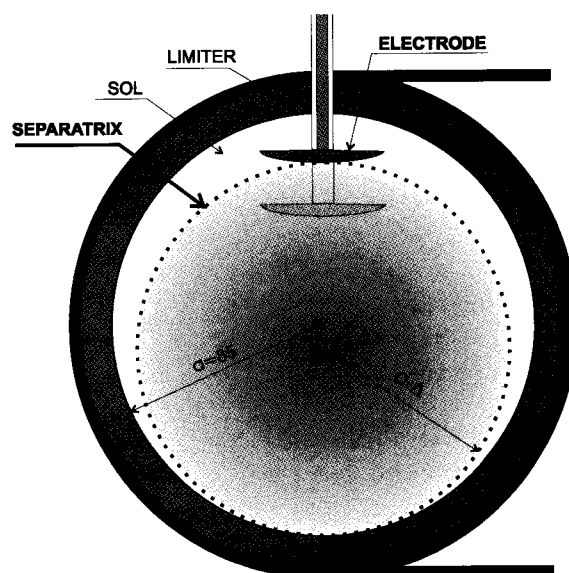

Fig. 1 Poloidal cross section of the CASTOR tokamak schematically showing the location of plasma column and biasing electrode at the "standard" and at the "separatrix biasing" arrangements, respectively.
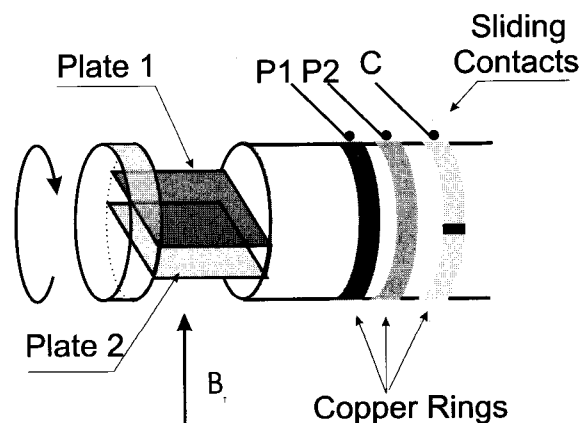

Fig. 2 Drawing of the rotating Mach probe.

3.1 Flow Measurements

The perpendicular and parallel flows are measured by a rotating Mach probe [7], which provides the first opportunity to study in detail the angular dependence of the ion flows with respect to the magnetic field lines, and to validate existing models [8]. The construction of the probe head is apparent from the schematic picture shown in Fig. 2. It consists of two back-to-back rectangular plates (3 *mm* × 5 *mm*), parallel to each other and spaced by 2 *mm* of insulating material. The probe head rotates by means of an electric drive located within the diagnostic port. The duration of one revolution is $T \geq 3$ *ms*, which determines the temporal resolution. The inclination of the plates is monitored by an auxiliary contact (C), which marks a defined angular position ($\theta_0 \doteq 29^o$). The probe is located at the top of the torus and radially movable on a shot-to-shot basis.

The temporal evolution of the ion saturation current measured by a plate during a single revolution provides its angular variation. A typical modulation of the probe signal is apparent from Fig. 3. The minima correspond to the orientation of the plate parallel to the magnetic field lines, while maxima are close to the perpendicular orientation.

There are fluid [7,9] as well as kinetic models [10] to interpret the ion collection by orientable probes in magnetized plasmas in the presence of perpendicular $E \times B$ drifts. In the following we will concentrate on the 2D kinetic model (PIC code), which has been adapted to simulate the CASTOR probe geometry. Rather than a cylindrical probe (circular boundary in the 2D plane),

two flat collectors separated by an insulator have been simulated. A comparison between experimental Mach probe data and PIC code results, displayed in Fig. 3, shows a good agreement over a large angular range.

3.2 2D Matrix of Langmuir Probes

The probe array consists of 64 tips arranged into 8 rows and 8 columns [4]. The distance between the rows, $d_r = 4.5$ *mm*, defines the radial resolution. The distance between the columns is $d_p = 6$ *mm*. The carbon tips (diameter 2 *mm*) are fixed in an insulating plate made of boron nitride. The individual tips measure either the floating potential or the ion saturation current. The mode of operation can be switched between shots. The data are digitized at a rate of 1 sample/μs.

The probe head itself is made of stainless steel, but covered by a layer of boron carbide (B_4C) to improve its compatibility with the plasma and to reduce its conductivity. The probe head is mounted on a manipulator allowing its radial motion on a shot-to-shot basis.

The position of the probe head in a poloidal plane of the CASTOR tokamak is shown schematically, but in scale, in Fig. 4. It is immersed into the edge plasma so that the magnetic field lines are perpendicular to the probe matrix, being located at the top of the torus (135° toroidally away from the ion side of the main poloidal limiter).

In the same figure, a snapshot of the distribution of the floating potential in the poloidal plane is shown as well. The dark regions in the plot denote the floating
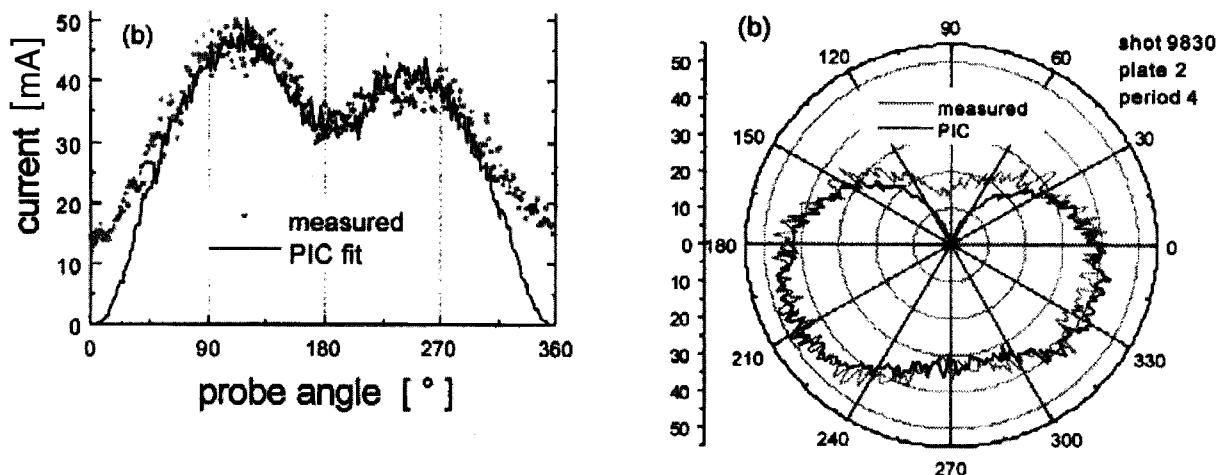

Fig. 3 Angular variation of the ion saturation current on a rotating plate – left. Polar diagram of the ion saturation current – right. Experimental data are fitted to the PIC model.
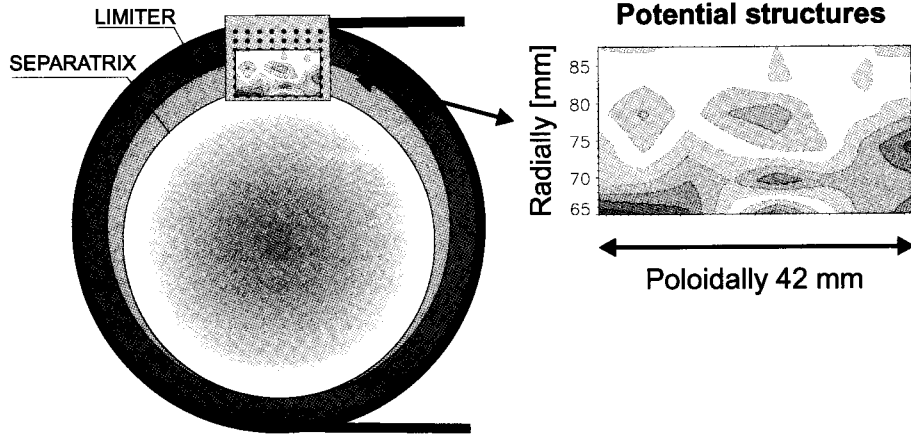
Fig. 4 Position of the 2D matrix in the poloidal plane of the CASTOR tokamak (in scale) together with a snapshot of potential structures. Only six rows of tips were active in this discharge.
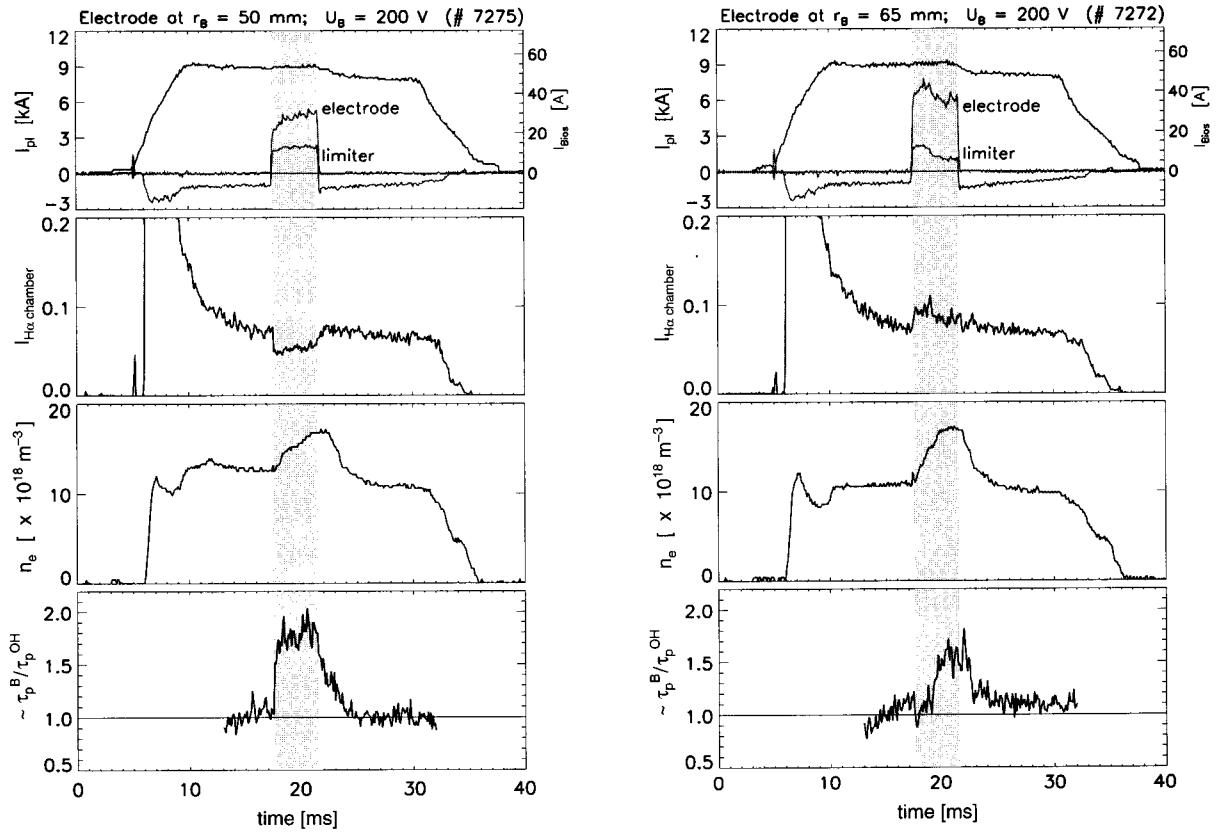

Fig. 5 Evolution of polarized discharges at "standard" (left) and "separatrix biasing" (right). From top to bottom: electrode current and return current to the poloidal limiter together with the evolution of the plasma current; intensity of the H_α spectral line; line averaged density; relative improvement of the global particle confinement time.

32

potential structures (potential valleys and hills) differing from the mean value. Even a visual inspection of such a map indicates that turbulent structures are smaller then the dimension of the array but larger then the distance between the tips. Pioneering research with a similar array was performed on the CALTECH tokamak [11].

The area of the probe head represents a non-negligible part of the the poloidal cross section. However, the radial profiles of the floating potential, measured at several radial positions of the probe head showed that the shadowing due to the array does not dominate the edge plasma.

4. Experimental Results
4.1 Evolution of Polarized Discharges

The evolution of the global plasma parameters at both the biasing schemes is compared in Fig. 5 for similar discharge conditions. The electrode is positively biased ($U_b = +200$ V).

As seen in Fig. 5, a current of about 35–40 A is drawn by the electrode during the biasing period. In spite of the different biasing configuration, the fraction of the electrode current flowing to the limiter is comparable.

The line averaged density increases substantially with biasing in both cases. However, the evolution of the H_α spectral line intensity I_{H_α} exhibits different shapes. For the "standard" configuration, the intensity drops immediately with biasing, which evidently implies a reduction of recycling and results in improvement of the global particle confinement (more than 50 %) [6]. On the contrary, at separatrix biasing, the H_α emission slightly increases during the initial phase of the biasing period. Nevertheless, the improvement of the global particle confinement time is of the same order as in the case of the standard biasing, as seen in the bottom panel of Fig. 5. However, for a precise comparison of particle confinement improvement, a detailed bookkeeping of recycling at the limiter, the wall and the electrode is required [1].

A substantial difference between the radial profile of the floating potential, U_{FL}, for both biasing schemes is apparent from Fig. 6. At "standard" biasing, the potential of the whole plasma column is shifted by $\sim U_b$ and, consequently, the radial electric field E_r is amplified between the electrode and the separatrix. On the other hand, at separatrix biasing, the potential is affected only in a relatively narrow region near the separatrix and the radial electric field is amplified at both sides of the electrode [4]. Consequently, the radial
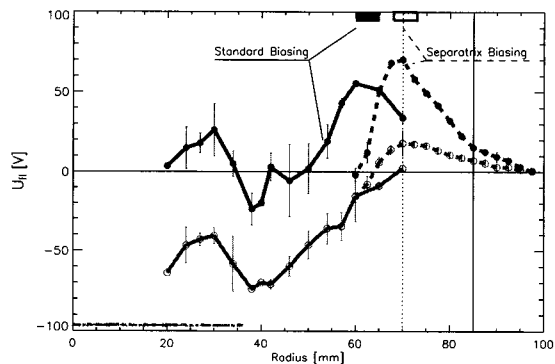

Fig. 6 Comparison of the radial profile of the floating potential with and without biasing ($U_b = +100$ V), plotted for two positions of the biasing electrode: $r_{bias} = 60$ *mm* – "standard" biasing scheme (solid lines), measured by a single floating probe on a shot-to shot basis; $r_{bias} = 68$ *mm* – "separatrix" biasing (dashed lines), measured by a rake probe.

electric field is highly sheared in that region and affects significantly the plasma flows and the turbulent structures. The strongest shear appears at the innermost side. The flow and fluctuation measurements described below have been performed with separatrix biasing.

4.2 Flow and Fluctuation Measurements in Sheared Electric Fields

Figure 7 shows radial profiles measured during separatrix biasing, ($U_b = +150$ V, the electrode position at $r = 70$ *mm*). The top panels show the potential/electric field profiles measured by the rake probe. The bottom panels show the parallel and perpendicular Mach numbers.

It is evident from the figure that the layers of the largest perpendicular flow velocity shear and the sheared region of the radial electric field appear to coincide ($r = 69 \div 72$ *mm*). Moreover, the values of the $E \times B$ shear rate, deduced from the radial electric field profile and the shear of the flow velocity v_{pol} derived from the $M_\perp$ profiles are comparable in this region

$$\Delta v_{E \times B}/\Delta r \approx \Delta v_{pol}/\Delta r \sim 5 \cdot 10^6 \ s^{-1}$$

and significantly exceed the typical growth rate of unstable modes. The growth rate is estimated from fluctuation measurements as the reciprocal value of the autocorrelation time, $\gamma = 1/\tau_A \sim 5 \cdot 10^4 \div 2 \cdot 10^5 \ s^{-1}$. It is worthwhile to note that the character of the electrostatic fluctuations in the edge plasma of CASTOR is similar to that observed in large – scale experiments [6].
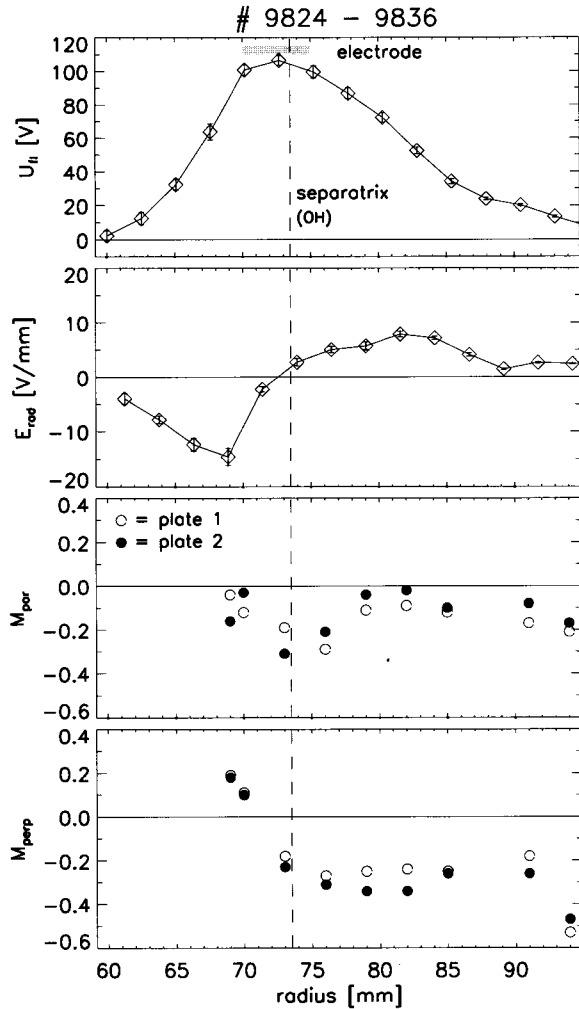
33

Fig. 7 Radial profiles at separatrix biasing (U_b = +150 V). Top panels: floating potential and radial electric field ($E_r = -\nabla U_{fl}$, neglecting ∇T_e with biasing). Bottom panels: parallel and perpendicular Mach numbers deduced from both plates (plate 1. – o, plate 2. – •). The dashed vertical line denotes the position of the separatrix in the non-polarized discharges.
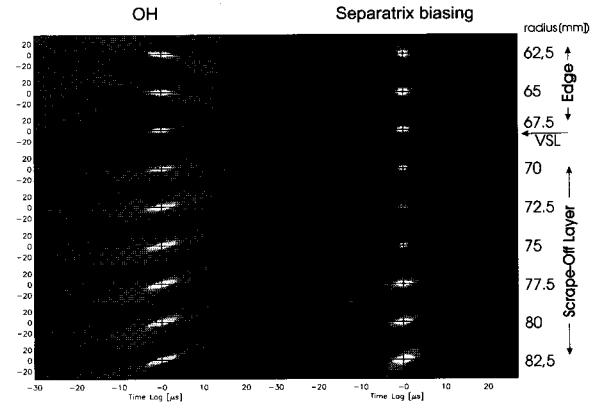

Fig. 8 Spatial-temporal correlation functions of the potential fluctuations in the poloidal direction for several radial positions of the poloidal probe array (indicated in the y-axis at the right hand side). Position of the separatrix – $r_s \doteq 67.5$ *mm*. Left column – ohmic phase, right column – polarized phase of the discharge (separatrix biasing, U_b = +150 V.

To demonstrate the strong impact of sheared flows on the edge turbulence, the data measured by the poloidal probe array was used [12,13]. The spatial-temporal correlation functions of potential fluctuations are calculated and the result is shown in Fig. 8, which consists of 18 panels. Each row of the figure corresponds to a single radial position of the probe array. The left panel of a row characterizes the turbulence in the OH phase of the discharge, the right one corresponds to the polarized phase (U_b = +200 V).

Each panel shows the spatial – temporal correlation

function. The bright patterns of elliptical shape are the regions of the highest correlation (> 50 %). Their dimension in the y-direction corresponds roughly to the poloidal extent of the turbulent structures ($\lambda_{pol} = 1 \div 2$ *cm*), while the x-dimension corresponds roughly to their lifetime ($10 \div 20$ μs). The poloidal propagation velocity of the structures is deduced from the slope of the correlation patterns. A more precise interpretation of such 2D correlation is given in [14].

The position of the separatrix is seen in the left column at $r = 67.5$ *mm*, where the reversal of poloidal propagation is well apparent. The biasing electrode is located approximately at the same radius. Thus, the region with the highest shear flow is formed there during biasing. A strong decorrelation of the turbulent structures in the poloidal direction as well as in time due to biasing is evident from a dramatic reduction of the size of the correlation patterns in this range of radii.

A similar effect is observed also in the radial direction [12,13] using the data from the rake probe. The simultaneous poloidal/radial correlation analysis at separatrix biasing (using data from the 2D matrix) is in progress [15].

5. Conclusions

The biasing arrangement and the plasma flow and turbulence measurements on CASTOR offered a first experimental proof that imposing a boundary condition by (non-intrusive) separatrix biasing is an efficient way

34

to create strongly sheared electric fields, thereby affecting plasma flows and decorrelating turbulent structures, and creating an edge transport barrier in the proximity of the separatrix, which leads to improved confinement.

The rotatable Mach probe enabled to measure the parallel and perpendicular plasma flows which are strongly affected in the sheared region, especially in the perpendicular direction. To improve the temporal resolution, especially for studying transient phenomena, a multi-pin Gundestrup system ([16], [8]) has been recently tested on CASTOR [17].

The $E \times B$ shear rate for separatrix biasing is larger than for standard biasing schemes, and significantly exceeds the growth rate of unstable turbulent modes. Probe array measurements demonstrated a strong impact on the turbulent structures.

Acknowledgement:

References

[1] R.R. Weynants *et al.*, Nucl. Fusion **32**, 837 (1992).

[2] V. Rozhansky and M. Tendler, *Reviews of Plasma Physics*, Vol. 19, ed. B.B. Kadomtsev (New York and London), 1996.

[3] G. Van Oost *et al.*, Czech. J. Phys. **50**, S3, 11 (2000).

[4] J. Stöckel *et al.*, *Proc. of 27th EPS Conf. Contrl. Fusion Plasma Phys.*, 2000, Budapest, p. 1032.

[5] M. Tendler, Plasma Phys. Contrl. Fusion **39**, B371, (1997).

[6] J. Stöckel *et al.*, Plasma Phys. Contrl. Fusion **41**, A577 (1999).

[7] K. Dyabilin *et al.*, *Proc. of 27th EPS Conf. Contrl. Fusion Plasma Phys.*, 2000, Budapest, p. 1653.

[8] J.P. Gunn *et al.*, Phys. Plasmas **8**, 1995 (2001).

[9] H. Van Goubergen *et al.*, Plasma Phys. Contrl. Fusion **41**, L17 (1999).

[10] J.P. Gunn, Czech. J. Phys. **48**, 293 (1998).

[11] S.J. Zweben and R.W. Gould, Nucl. Fusion **25**, 171 (1985).

[12] J. Stöckel *et al.*, *26th EPS Conf. Contrl. Fusion Plasma Phys.*, 1999, Maastricht, p. 1589.

[13] J. Stöckel *et al.*, J. Tech. Phys. **41**, Special Issue, 49 (2000).

[14] J. Petrzilka and J. Stöckel, Control. Plasma Phys. **38S**, 74 (1998).

[15] E. Martines *et al.*, *to be published in Proc. of 28th EPS Conf. Contrl. Fusion Plasma Phys.*, 2001, Funchal.

[16] C.S. MacLatchy *et al.*, Rev. Sci. Instr., 3923 (1992).

[17] J.P. Gunn *et al.*, *to be published in* Czech J. Phys., **51**, 1001 (2001).